Quantum-Network Nodes with Real-Time Noise Mitigation Using Spectator Qubits

S.J.H. Loenen,[1,2,*] Y. Wang,[1,3,*] N. Demetriou,[1,2] C.E. Bradley,[1] and T.H. Taminiau[1,2,†]

[1] *QuTech, Delft University of Technology, P.O. Box 5046, Delft 2600 GA, The Netherlands*

[2] *Kavli Institute of Nanoscience Delft, Delft University of Technology, P.O. Box 5046, Delft 2600 GA, The Netherlands*

[3] *3rd Institute of Physics, University of Stuttgart, Allmandring 13, Stuttgart 70569, Germany*

(Received 20 May 2025; revised 12 November 2025; accepted 13 January 2026; published 10 April 2026)

Quantum networks might enable quantum communication and distributed quantum computation. Solid-state defects are promising platforms for such networks, because they provide an optical interface for remote entanglement distribution and a nuclear-spin register to store and process quantum information. A key challenge toward larger networks is to improve the storage of previously generated entangled states during new entanglement generation. Here, we introduce a method that uses "spectator" qubits combined with real-time decision making and feedforward to mitigate dephasing of stored quantum states during remote entanglement sequences. We implement the protocol using a single nitrogen-vacancy (NV) center in diamond and demonstrate improved memory fidelity. Our results show that spectator qubits can improve quantum network memory using minimal overhead and naturally present resources, making them a promising addition for near-term testbeds for quantum networks.

DOI: 10.1103/zgm8-6b8l

I. INTRODUCTION

Quantum networks hold promise for a multitude of applications, ranging from secure communication and quantum sensor networks to distributed quantum computation [1–5]. A potential architecture consists of quantum nodes that each contain a qubit register that provides quantum processing power, including quantum memory, and an optical interface to establish entangled links between different nodes [6]. The nitrogen-vacancy (NV) center in diamond, like other solid-state defects in wide-bandgap semiconductors [7–11], provides these elements. The electronic spin can be interfaced with photonic qubits so that entanglement can be established [12,13]. In addition, the defect host material provides long-lived nuclear-spin qubits that can be used as robust quantum memories as well as processing qubits via their interaction with the electronic spin [14].

Following pioneering work on two-node quantum networks in different platforms [13,15–17], currently the largest quantum network able to run quantum protocols, such as entanglement swapping and quantum teleportation, consists of three solid-state defect nodes [7,18]. To efficiently create larger networks, it is desirable to faithfully store previously generated entangled states while generating new entangled links. Nuclear-spin qubits provide a robust memory. However, in network demonstrations to date, their decoherence rate under entanglement generation is still larger than the rate at which new entangled states are generated [7,19], which is captured by an active link efficiency smaller than 1 [20]. On the one hand, a substantial amount of work is dedicated to improving the entanglement generation rate by incorporating defects into cavities [8,21–23]. On the other hand, the memory has been made more robust against entanglement generation attempts by optimization of the entanglement generation process [7, 24], as well as by reducing the effective coupling of the memory to the noise [20,25,26].

This work introduces a complementary approach to protect the quantum network memory, which is based on sensing the noise experienced by the memory qubit during entanglement generation using auxiliary "spectator" qubits [27–34]. The underpinning idea is that the spectator qubits sense the noise process of interest, so that real-time feedforward, in combination with knowledge of how noise on the spectators correlates to the noise on the memory qubit, enables mitigation of the loss of quantum information stored in that memory qubit.

*These authors contributed equally to this work.

†Contact author: T.H.Taminiau@TUDelft.nl

A key difference with respect to other methods, such as decoherence-protected subspaces or quantum error correction [25,35], is that the spectator qubit approach does not require the encoding of the memory qubit in an entangled state before the noise process acts, thus reducing overhead and the associated initial loss of fidelity. Instead, the decision to act on the information accumulated on the spectators can be made dynamically after the noise process has acted. In cases where little noise was created, for example because the remote entanglement generation succeeded early, the operations on the spectators can be omitted, thereby avoiding the associated overhead and dephasing. Conversely, if remote entanglement generation induced significant noise, the spectators are used and reduce the total dephasing. Related approaches with spectator qubits have previously been proposed for real-time system calibration in trapped-ion qubits [27], for monitoring energy injection events in superconducting qubits [28] and inspired work on photonic spectator modes. Experimentally, spectator qubits have been implemented for mid-circuit error correction in dual-species cold atom arrays [29].

In this work, we investigate the spectator qubit approach in a quantum network setting, as demonstrated in Fig. 1. We demonstrate that the usage of multiple spectator qubits can extend the coherence time of a quantum memory during a control sequence that emulates remote entanglement generation. We use a NV center as a quantum node, where the nuclear-spin register provides a quantum memory and multiple spectators. The electronic spin of the NV center serves as an optical interface to emulate the distribution of entanglement over different nodes, as well as to initialize, measure and control the nuclear spins. During the probabilistic entanglement generation sequence, the electron spin undergoes stochastic evolution, which, due to the always-on electron-nuclear hyperfine coupling, imposes spatially correlated dephasing on the memory and spectator qubits [25,36]. Since no entangled state has to be created between spectator and memory qubits, spectator qubits provide additional noise information with minimal extra operations on the memory qubit and the associated fidelity loss. This approach is complementary to other methods such as quantum error correction or decoherence-free subspaces, where the memory qubit is encoded in an entangled state forming a logical qubit.

Furthermore, we investigate different strategies for using the spectator qubits. First, we demonstrate that the overhead required to extract the spectator information imparts noise onto the system of interest and hence defines a trade-off as to when it is beneficial to access spectator qubits. Then we identify the measurement of the spectator qubits as one of the main noise sources and mitigate this by employing a gate-based (without mid-circuit measurements) implementation. Based on these results, we show which spectator strategies to use given an entanglement success probability per entanglement generation trial. These results indicate that employing nuclear spins as spectator qubits provides a viable path to extend the memory coherence time when the noise experienced by the nuclear spins is dominantly correlated.

II. BAYESIAN INFERENCE OF THE PHASE

We investigate the spectator qubit approach in a well-characterized NV system described by Abobeih *et al.* [37]. The NV electronic spin couples to a register of nuclear-spin qubits, of which the dynamics are described by

$$H_{n_i} = \omega_l I_z \otimes |0\rangle\langle 0|_e + \left[(\omega_l - A_{\parallel_i})I_z + A_{\perp_i} I_x\right] \otimes |1\rangle\langle 1|_e , \quad (1)$$

where "i" labels each single nuclear spin, ω_l is the nuclear-spin qubit Larmor frequency, $\{A_\parallel, A_\perp\}$ the hyperfine coupling parameters to the electron-spin qubit and $|m_s\rangle_e$ denotes the electron-spin state ($|0\rangle$, $|1\rangle$ corresponding to the $m_s = 0, -1$ projections, respectively). For sequences with stochastic electron-spin evolution (such as investigated in this work), the hyperfine interaction introduces decoherence on the nuclear-spin qubits.

To provide insight into the spectator qubit approach, as an example, we first consider the limit where $A_{\perp_i}/(\omega_l \pm A_{\parallel_i}) \ll 1$ (i.e., a high magnetic field regime). In this case, the two electron-spin-conditioned nuclear-spin dynamics in Eq. (1) commute (Sec. I in the Supplemental Material [38]), resulting in decoherence that manifests purely as dephasing. Furthermore, the correlation of the phase evolution of different nuclear-spin qubits is then set by their parallel hyperfine components $A_\parallel$.

Measurements on the spectator qubits reveal these correlations and facilitate a Bayesian update (Sec. II in the Supplemental Material [38]) of the memory qubit's phase distribution according to the likelihood function,

$$P(\phi \mid \mathcal{M}_n) \propto \prod_{i=1}^{n} \frac{1 + (-1)^{m_i}\cos(g_i\phi - \theta_i)}{2} P_0(\phi). \quad (2)$$

Here $P(\phi|\mathcal{M}_n)$ is the memory (or spectator) qubit phase distribution given a string $\mathcal{M}_n$ of n spectator readout outcomes m_i, with $m_i \epsilon \{0, 1\}$. $g_i = A_{\parallel_i}/A_{\parallel_m}$ is the ratio of the parallel hyperfine couplings of spectator i ($A_{\parallel_i}$) and the memory qubit ($A_{\parallel_m}$), θ_i denotes the basis in the XY plane of the Bloch sphere along which spectator i is read out, and $P_0(\phi)$ is the memory-qubit phase distribution prior to any spectator measurements. Figure 1(b) provides a graphical representation of spectator-measurement-induced phase narrowing of the memory qubit.

Equation (2) also gives the updated phase distribution of any not-yet-measured spectator qubits. Figures 1(c) and 1(d) exemplify the narrowing of the memory-qubit phase

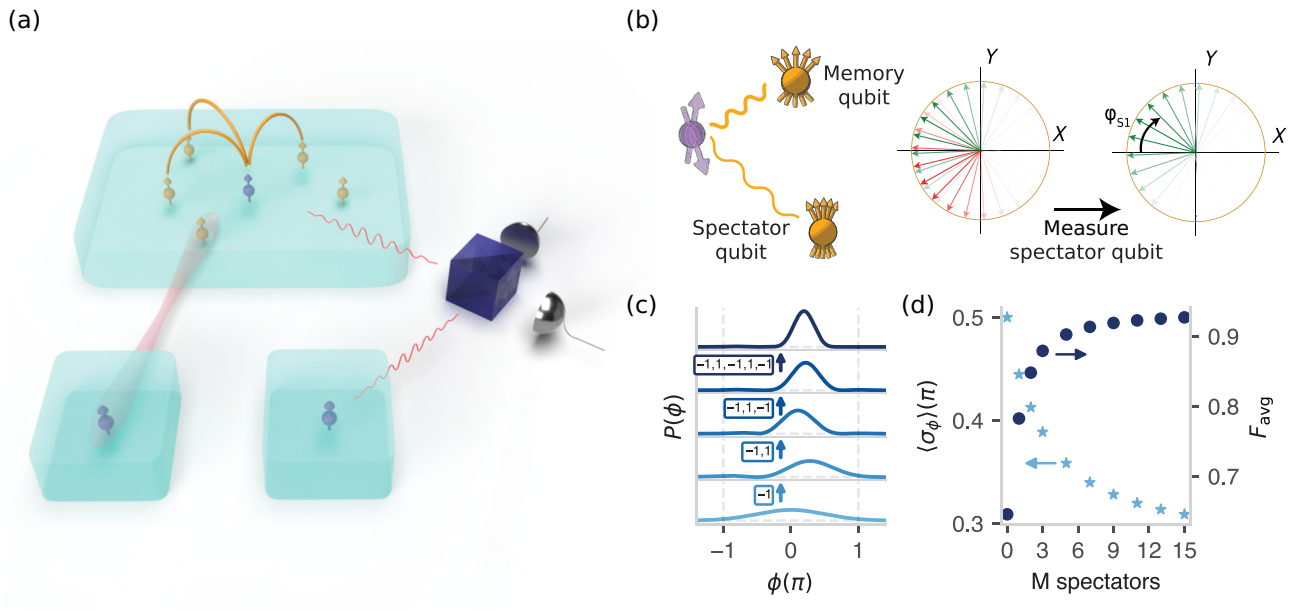

FIG. 1. Concept: spectator qubits for network nodes. (a) Schematic of the spectator qubit protocol in a quantum network setting. Blue blocks indicate separate network nodes that each hold a communication qubit (purple) that is used as an optical interface. Additional qubits (only drawn in one node) interact with the communication qubit and can serve different purposes, such as memory qubit (hold previously generated entangled state), idle qubit (store newly generated entangled state) or spectator qubits (provide information on memory-qubit dephasing, indicated with yellow half circles connected to the communication qubit). (b) Example of correlated noise between the memory and spectator qubit. The arrows and their opacity reflect the phase probability density function. (left circle) The complete memory-qubit phase distribution before the spectator readout consists of the weighted sum of the memory-qubit phase distributions conditioned on a spectator qubit measurement outcome in orthogonal measurement bases in the XY plane (along the $+Y$ axis, green, or the $-Y$ axis, red). (right circle) Memory-qubit phase distribution after the spectator qubit is measured in the $+Y$ axis. (c) Narrowing of the memory-qubit phase probability density distribution for a specific readout syndrome of M spectators. Here we set $A_\perp = 0$ and take $A_\parallel$ to be identical for all qubits ($g_i = 1$). For $M = 0$, the state of the memory (and each spectator) qubit is $|\psi\rangle = \frac{1}{2}\left[|0\rangle + e^{-i\phi}|1\rangle\right]$, with $P_0(\phi) = \frac{1}{\sigma\sqrt{2\pi}} \exp\left(-\frac{1}{2}(\phi^2/\sigma^2)\right)$ and $\sigma = \frac{1}{2}\pi$. As an example, we consider the case with readout outcomes $m_i = 1$ for the even-numbered spectator qubits and $m_i = 0$ for the odd ones. Therefore, the center of the spectator-updated phase distribution alternatively shifts left and right [see, e.g., the red ($m_i = 0$) and green ($m_i = 1$) spectator-updated phase distributions in (b)]. In this calculation, gates and measurements are ideal. (d) Standard deviation $\langle\sigma_\phi\rangle$ of the memory-qubit phase distribution averaged over all possible spectator readout outcomes, and the corresponding memory-qubit fidelity F_{avg}.

distribution, and corresponding improved fidelity, after measuring M spectators, where each spectator is measured in a basis perpendicular to its predicted Bloch vector (Sec. III in the Supplemental Material [38]). Note that, even in this idealized case, extending to a general analytical scaling for more spectator qubits is nontrivial, as it requires averaging equation (2) over all spectator measurement syndromes, and each θ_i itself is a function of equation (2) for $i - 1$ spectator qubits.

III. SPECTATOR QUBITS IN ENTANGLEMENT PROTOCOLS

We apply this approach in an experimental setting where we emulate a sequence of N_{REA} remote entanglement attempts after initializing M spectator qubits in the X-basis, see Fig. 2(a) with $M = 2$. Here, a single entanglement attempt consists of a stochastic electron-spin reset, the preparation of a superposition state on the electron-spin qubit and a waiting time t_e that, for example, allows the heralding signals of entanglement to be received before the next electron-spin reset. Note that we, as in previous studies [20,39], omit the optical π-pulse to generate spin-photon entanglement due to hardware limitations, and that various other sequences and protocols are possible, including adding extra pulses on the electron spin [7,13,40]. The case studied here results in predominantly correlated noise and therefore is an interesting example to illustrate the principle of spectator qubits; the exact performance will depend on the parameters of a given system and sequence, and the resulting noise correlations. To rephase quasi-static noise, we implement a nuclear-spin echo after half the entanglement attempts.

The electron-spin evolution during the reset depends on the optical cycling of the electronic spin, where stochastic decays occur from the excited state directly, or through the meta-stable state, to the ground state [10,39]. In addition, the reset projects the superposition state. Over many

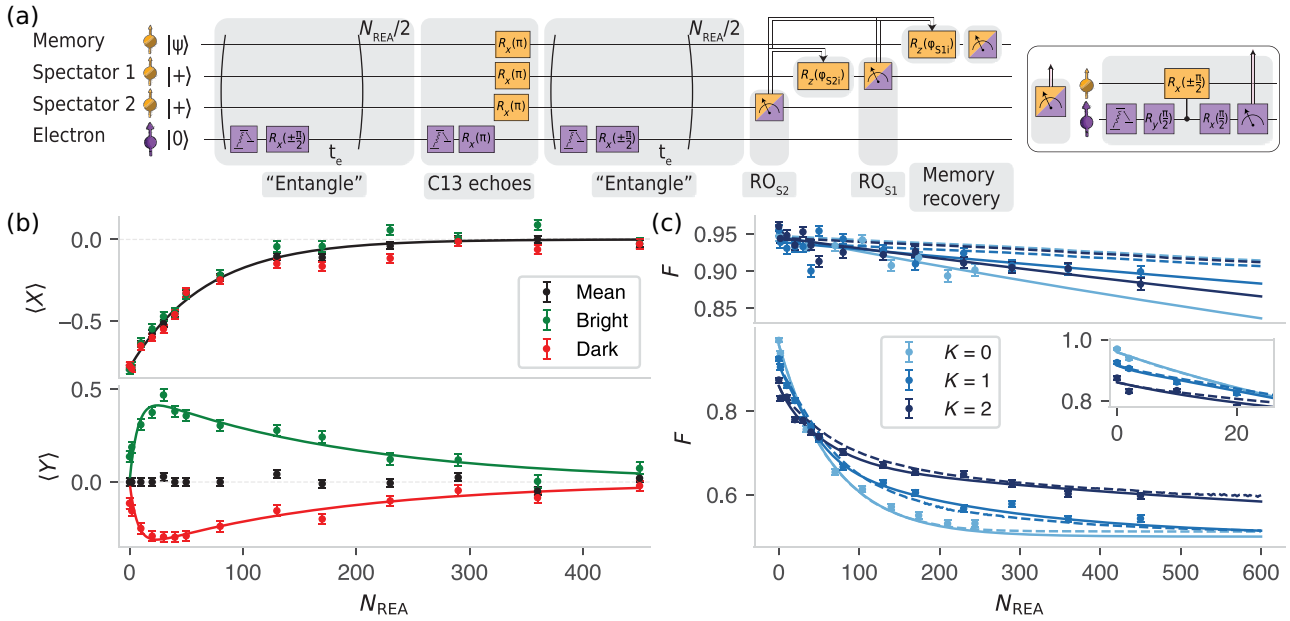

FIG. 2. Spectator-based real-time noise mitigation. (a) Experimental sequence with $M = 2$ spectator qubits. After N_{REA} entanglement attempts, K spectators are read out ($K = M = 2$ in the sequence shown). To maximize the information gain, the readout basis of each spectator [set by a $R_Z(\phi)$ rotation], is determined in real-time by the combined measurement syndrome of previously read out spectators (see Sec. III in the Supplemental Material [38]). The boxed inset shows the underlying gate sequence for the spectator-qubit readout, where the two-qubit gate involves dynamical decoupling on the electron-spin qubit. (b) Experimental data of the evolution of the memory qubit $\langle X\rangle$ and $\langle Y\rangle$ after running the protocol in (a) with the memory qubit initialized in the $|{+}X\rangle$ state and a spectator with $g = 1.49$. Data are conditioned on obtaining a bright (green) or dark (red) readout on the first spectator. Black data are unconditioned. (c) Fidelity F of the final state after the protocol in (a). (top) Memory qubit initialized in $|0\rangle$. (bottom) Average over data with memory-qubit initial states in $|{+}X\rangle$ and $|{+}Y\rangle$ for different number of spectator qubits initialized and read out. For low N_{REA}, the measurement of the spectators imparts more dephasing noise on the memory qubit than the amount of dephasing that is compensated (see inset). Solid lines are fits and dashed lines are simulations (see Secs. IV and VI in the Supplemental Material [38]).

entanglement attempts, these processes generate dephasing on the nuclear-spin qubits, which is correlated by the nuclear-spin hyperfine parameters.

In an actual setting, upon completion of all N_{REA} attempts, the state of the electronic spin would be transferred to an idle nuclear-spin qubit to free up the electron spin for subsequent spectator qubit readouts. As we focus on the dephasing process and do not generate an entangled state between different nodes, such a step is omitted in this work. Therefore, at the end of the emulated entanglement generation sequence, we reset the electron spin and read out $K \leq M$ spectators sequentially via the electron-spin qubit. As with other noise mitigation protocols that involve nuclear-spin qubits gates (order ~ 1 ms, similar to order $100\,N_{\mathrm{REA}}$), the spectator protocol increases the protocol time to protect precious previously generated quantum states. Metrics for well-performing spectator qubits are good gate fidelities (typically by having sufficiently dissimilar hyperfine components, noting that even $|g| = 1$ can be achieved using opposite signs [25]), small $A_\perp$ compared to the Larmor frequency (reducing noncommutivity, Sec. I in the Supplemental Material [38]) and a range of g-values depending on the expected dephasing (Sec. IV in the Supplemental Material [38]). Solely considering a nuclear-spin environment, these aspects are approximately concentration independent and typically yield order a handful of potential spectator qubits. Note that we can decide in real time how many spectators we read out. This allows one to only measure a spectator at the end of the entanglement generation process if this will improve the coherence of the memory qubit, which can be calibrated in advance [see discussion below and Fig. 2(c)]. Each spectator readout basis is set in real time based on the measurement outcomes of previously measured spectators.

We now experimentally demonstrate spectator-qubit-induced phase narrowing. First, we perform an experiment using two nuclear spins labeled C0 and C1 with respective hyperfine parameters $\{A_\parallel, A_\perp\}$ given by $\{24.4, 24.8\}$ and $\{-36.3, 26.6\}$ kHz [37]. All data are taken with a magnetic field of 404 G along the NV symmetry axis. We execute the sequence in Fig. 2(a) with C0 as the memory qubit (initialized in $|{+}X\rangle$, $|{+}Y\rangle$ or $|0\rangle$) and C1 as spectator 1 (always initialized in $|{+}X\rangle$) ("spectator 2" is not used). The dephasing on both qubits is correlated via

their hyperfine parameters ($A_\parallel$) and increases for increasing N_{REA} (longer stochastic electron evolution). At the end of the sequence, we measure the memory qubit [$\langle X\rangle, \langle Y\rangle$, Fig. 2(b)]. Conditioned on the spectator qubit readout in the $-Y$ basis (labeled as "bright" or "dark," for electron-spin states $m_s = 0$ and $m_s = -1$, respectively), we observe a projection of the memory qubit either toward the $+Y$ or $-Y$ basis, demonstrating the correlation.

We now include a second spectator qubit C2 ($\{A_\parallel, A_\perp\} = \{20.6, 41.5\}$ kHz). Correspondingly, the g-values of the spectator qubits are $g_{C1} = -1.49$ and $g_{C2} = 0.84$. The readout axis of the second spectator qubit can now be calibrated, given the readout syndrome on the first spectator, to be perpendicular to its predicted Bloch vector. To quantify the corresponding reduction of dephasing on the memory qubit, we consider the fidelity associated with the remaining memory-qubit coherence: $F = \frac{1}{2}\sqrt{\langle X\rangle^2 + \langle Y\rangle^2 + \langle Z\rangle^2} + \frac{1}{2}$, as shown in Fig. 2(c).

For larger N_{REA} (increased dephasing), we observe a marked improvement in the final fidelity when using additional spectator qubits. Conversely, for small N_{REA} (i.e., no or limited dephasing), adding spectators reduces the fidelity due to the additional dephasing introduced by the operations on the spectators (see below), which is independent of the number of N_{REA}.

Because phase is a 2π cyclic variable, correlation between the spectator and memory-qubit phase is a nontrivial function of the g-value (see Secs. IV and VI in the Supplemental Material [38]). For small memory-qubit dephasing, an absolute value of g larger than 1 is desired as this provides better contrast upon measuring the correlated phase on the spectator qubit. However, for larger memory-qubit dephasing an absolute value of g close to 1 is more optimal as it prevents a 2π wrapping of the phase difference between the memory and spectator qubit. This explains the more significant improvement of spectator 2 compared to spectator 1 for large N_{REA}, where a g-value closer to 1 is more optimal. Memory-qubit eigenstates along the Z-axis show a limited loss of fidelity (bit flips), confirming that the dominant process is dephasing. The spectator qubits approach implemented here is tailored to dephasing noise and does not protect the Z-basis states. We confirm our understanding by comparing the experimental data set with a simulation that models the sequence shown in Fig. 2(a). See Sec. VI in the Supplemental Material [38] for a detailed discussion on the simulation.

Imperfections in the spectator-qubit control and readout reduce the overall performance through two distinct mechanisms. The spectator readout consists of first mapping the spectator-qubit state to the electron-spin qubit, upon which the electron is state-selectively optically cycled for state determination via photon detection. First, a faulty spectator measurement outcome (e.g., an initialization or readout error) leads to an incorrect phase update of the memory qubit, reducing the net gain from the spectator qubit. Second, stochastic electron spin flips during the spectator readout (e.g., the electron started in the bright state, but flipped to the dark state during optical cycling prior to photon collection) lead to an additional unknown phase on the nuclear-spin qubits, causing additional dephasing (Sec. V in the Supplemental Material [38]). Hence, measuring a spectator is only desired if the net information gain outweighs the additional measurement-induced dephasing. While the additional dephasing is independent of the number of entanglement attempts N_{REA} executed, the information gain from spectator measurements depends on N_{REA}. Consequently, the optimal strategy related to which spectators to read out depends on N_{REA}, which is demonstrated in Fig. 2(c). For low N_{REA}, see inset, the strategies involving spectator qubits provide a lower memory fidelity compared to those that do not use spectators.

In the following, we present a gate-based implementation that bypasses the need for readout of spectator qubits.

IV. GATE-BASED SPECTATOR QUBIT IMPLEMENTATION

Unlike previously considered applications of spectator qubits [27–30], our system naturally provides controlled two-qubit interactions between the spectator/memory qubits and the source of dephasing (the electron-spin qubit). This enables us to efficiently replace the measurement-based scheme with a gate-based scheme, by substituting the measurement and classical feedforward by an equivalent two-qubit gate and qubit reset. We now explain the gate-based implementation in detail.

After N_{REA} repetitions of the remote entanglement sequence, we prepare the electron-spin qubit into an eigenstate. The goal is to (partly) revert the (unknown) phases picked up by the nuclear-spin qubits. To achieve this, we take two steps. First, we implement a spectator-controlled electron bit flip that correlates a $+(\pi/2)$ ($-(\pi/2)$) spectator phase [in the nuclear spin rotating frame with frequency $f_r = \frac{1}{2}(f_{|0\rangle_e} + f_{|1\rangle_e})$, the average over the two electron-spin-dependent nuclear-spin frequencies] with the electron state that induces a negative (positive) phase on that spectator [right panel of Fig. 3(a)]. Second, we apply a waiting time δ_t, which creates an electron-controlled phase rotation on all nuclear spins.

Because the imparted phases are set by the same couplings ($A_{\parallel i}$) as those that created the dephasing, all nuclear spins can be refocused simultaneously. The efficiency of the phase reversal depends on correctly timing δ_t [Fig. 3(b) and Sec. VIII in the Supplemental Material [38]]. A too long δ_t overcompensates the obtained unknown nuclear-spin qubit phase and therefore effectively imparts additional dephasing.

We experimentally demonstrate this in Fig. 3(c), where we plot the Bloch vector length (BVL) given by

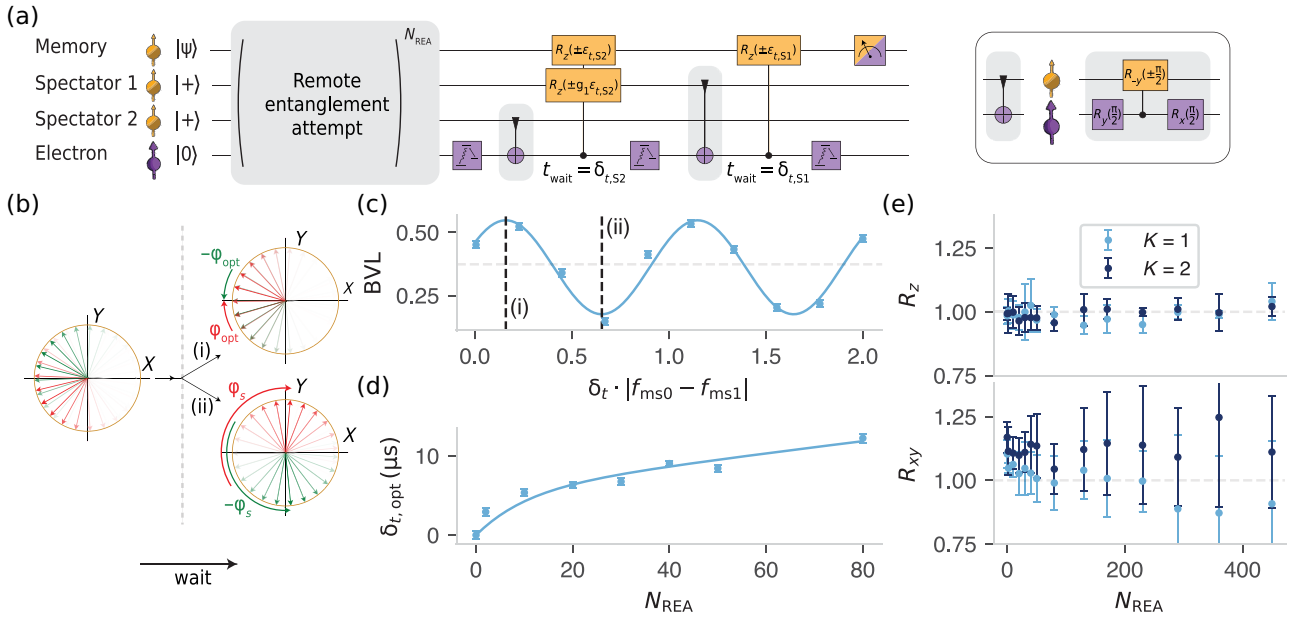

FIG. 3. Gate-based spectator implementation. (a) Experimental sequence. Before memory retrieval, the state of a spectator qubit is mapped to the electron-spin qubit and a waiting time is applied that implements an electron-controlled $R_Z(\theta)$ operation on all nuclear-spin qubits (Sec. VII in the Supplemental Material [38]). Since the electron state is correlated with the phase of a spectator qubit, all nuclear spins that experienced correlated noise partly rephase if the interaction time is correctly set, see (b). The use of multiple spectators provides an accumulated rephasing. The boxed inset shows the underlying gate sequence for the spectator-controlled electron flip. (b) (left) Memory-qubit phase distribution after mapping the Y-basis expectation value of a spectator qubit to the electron-spin Z-basis (red (green) phase distribution correlates with the $|0\rangle$ ($|1\rangle$) electron-spin state). (right) Upon applying a waiting time δ_t, the two distributions acquire electron-spin-dependent conditional phase. By timing optimally, the distributions pick up a phase $\pm\phi_{\text{opt}}$ and maximum rephasing occurs (top). Suboptimal timing provides a phase $\pm\phi_s$ and can induce further dephasing (bottom). (c) Experiment with $N_{\text{REA}} = 30$, C0 as the memory qubit and one spectator qubit (C1). The memory-qubit Bloch vector length with sinusoidal fit as a function of the waiting time after the nuclear-spin-conditioned electron rotation, (i) and (ii) correspond to the optimal and suboptimal rephasing times [see (b)]. (d) The optimal rephasing time $\delta_{t,\text{opt}}$ as a function of N_{REA} (Sec. IV A in the Supplemental Material for fit [38]). (e) Quantification of the improvement of the gate-based implementation over the measurement-based implementation. Data are averaged over all permutations of C0, C1 and C2 acting as memory and spectator qubits, see Sec. XI in the Supplemental Material [38]. We plot the ratio of the memory-qubit Bloch vector length for the memory qubit initialized in $|0\rangle$ (R_z, top) and averaged over the memory-qubit initial states $|+X\rangle$ and $|+Y\rangle$ (R_{xy}, bottom). The vertical bars represent the standard deviation of the underlying distribution from which R_z and R_{xy} are calculated (not the statistical error on the mean value). No effect is observed in the R_z, while a considerable improvement is observed in R_{xy} for the gate-based scheme.

$\sqrt{\langle X\rangle^2 + \langle Y\rangle^2 + \langle Z\rangle^2}$ for different δ_t. The best waiting time $\delta_{t,opt}$ corresponds to the first maximum, because only at this time all nuclear-spin qubits optimally rephase simultaneously. Timings of subsequent maxima, which are possible because of the 2π cyclicity of the phase, depend on the specific hyperfine couplings of individual nuclear spins (spectators as well as memory qubits). More entanglement attempts (larger N_{REA}) will induce more stochastic dephasing and correspondingly require a longer waiting time δ_t to achieve optimal phase reversal [Fig. 3(d)]. A challenge arises for nuclear-spin states that did not undergo the dephasing process during entanglement generation. For example, the nuclear spin to which a potential heralded entangled state is swapped actually dephases during the waiting time δ_t. However, because the electron-spin state is now controlled rather than stochastically fluctuating, this additional dephasing can be resolved through an echo pulse at $\frac{1}{2}\delta_t$ on those nuclear spins.

We now implement the gate-based approach in the sequence of Fig. 3(a), where we have calibrated $\delta_{t,S2}$ and $\delta_{t,S1}$ for both spectators, and compare this to the measurement-based implementation of Fig. 2. We compare the two approaches by implementing the two schemes for different permutations of C0, C1 and C2 (memory or spectator qubits, see Sec. XI in the Supplemental Material [38] for the complete dataset).

For each permutation, we measure the ratio R of the gate-based BVL over the measurement-based BVL after N_{REA} entanglement generation sequences and with K spectator qubits. Subsequently, for different initial states of the memory qubit, we plot the average R obtained over the different permutations, together with the standard deviation of the underlying distribution [Fig. 3(e)].

When the memory qubit is initialized in an eigenstate, the ratio (R_z) remains close to 1. In contrast, when initialized in $|+X\rangle$ or $|+Y\rangle$, the ratio R_{XY} is larger than 1 (for most, but not all permutations). Note that data points closer to $N_{\mathrm{REA}} = 0$ provide a better representation of the gate- vs measurement-based scheme, as for large N_{REA}, and hence (nearly) completely dephased states, R_{XY} is more dominated by measurement noise, and that for constant entanglement success probability low N_{REA} is more probable (see Sec. V). These results confirm that the gate-based implementation provides an improvement over the measurement-based approach.

V. OPTIMAL STRATEGY FOR DIFFERENT SUCCESS PROBABILITIES

We now analyze what the optimal number of spectators is for a given probabilistic entanglement generation process. We consider a probability p to successfully generate entanglement in each attempt. The likelihood for success at attempt N_{REA} is then given by $P(N_{\mathrm{REA}}) = (1-p)^{N_{\mathrm{REA}}-1} \cdot p$. We analyze the use of spectator qubits as a function of p by considering what the expected fidelity ($\overline{F} = \sum_{N_{\mathrm{REA}}=1}^{\infty} F(N_{\mathrm{REA}}) \cdot P(N_{\mathrm{REA}})$) of the memory qubit is with respect to its initial state. $F(N_{\mathrm{REA}})$ is the memory-qubit fidelity at attempt N_{REA}.

We investigate and execute the gate-based implementation with the spectator and memory qubits identical to the ones used in Fig. 2(c). We consider the situation where, after completion of N_{REA} entanglement sequences, we use the phase-information contained in each spectator that was initialized. Furthermore, we analyze the cases with 0, 1 or 2 spectators initialized. Figure 4(a) shows the memory fidelity F averaged over datasets with the memory qubit initialized in the X-, Y- and Z-basis. In addition, we have analyzed datasets with the memory qubit initialized in the $-Z$-basis, which showed no significant difference from data with the memory qubit initialized in the $+Z$-basis. We fit the data using the analytical result for using a single spectator (Sec. IV in the Supplemental Material [38]), where we fix the state preparation and measurement (SPAM) error such that the fit overlaps with the data at $N_{\mathrm{REA}} = 0$. Using these fits, we interpolate the data and calculate $\overline{F}$.

For low entanglement success probability p, there is a relatively high likelihood to generate entanglement at large N_{REA}, where using spectators considerably outperforms not using spectators [Fig. 2(c)]. This explains the regime in Fig. 4(b) where using spectators ($K \neq 0$) outperforms using no spectators. On the contrary, for $p \approx 1$, low numbers of N_{REA}, where little correlated noise is built up, dominate $\overline{F}$. Therefore, at low N_{REA}, using spectators is not expected to provide a significant improvement over not using spectators. Rather, spectator-induced overhead can lower $\overline{F}$ at low N_{REA}.

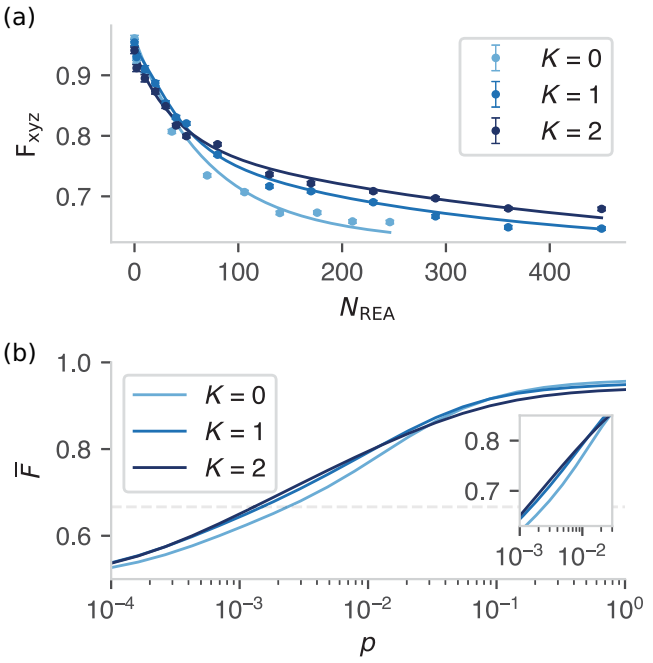

FIG. 4. Memory fidelity F for different entanglement generation success probabilities using spectator qubits. (a) Memory fidelity F after N_{REA} entanglement generation attempts in the gate-based implementation using K spectators, averaged over the memory initial states $|0\rangle$, $|+X\rangle$ and $|+\mathrm{Y}\rangle$. (b) Using the fits [solid lines in (a), see Sec. IV in the Supplemental Material [38]], we plot the expected average memory-qubit fidelity ($\overline{F}$, main text) for different number (K) of spectators used.

A further optimization strategy, which is not implemented here, is to decide in real time, for each spectator and based on N_{REA} until success for that instance, to use the information contained or not, i.e., to apply the measurement- or gate-based scheme. As the spectator qubit initialization comes at little costs (Fig. 3 in the Supplemental Material [38]), an optimal strategy could be to always initialize multiple spectators and then decide which ones to use based on the number of sequence repetitions until success. This would approximately follow the highest values of the curves in Fig. 4(a). Besides a longer required system initialization time, the cost of using more spectator qubits is an increased one-time (numerical or experimental) calibration cost of spectator readout angles (measurement-based) or electron wait times (gate-based). Finally, we note that the spectator approach enables using qubits with limited fidelities, which might not be suitable to serve other purposes, as one can always decide at the end of the sequence to not use a spectator unless the dephasing was strong enough that it will improve memory-qubit fidelity.

VI. CONCLUSION AND OUTLOOK

In this work, we used an NV center in diamond to demonstrate a method that uses multiple spectator qubits

to mitigate the dephasing of quantum states stored in a quantum network node under an emulated entanglement process. This approach relies on the sensing of correlated noise along one axis, so that measurements performed on the spectator qubits reveal partial information of the noise imposed on the memory qubit. For other types of systems and entanglement sequences, such as those including echo-pulses on the electron spin [7,12,41], the type of noise and its degree of correlations can vary, increasing or decreasing the effectiveness of spectators.

Advantages of the spectator approach are: (1) it can be combined with other methods; (2) it imparts little intrinsic overhead or fidelity loss in preparation, as entanglement between the spectator qubits and the memory qubit is not required; (3) it can make use of qubits with limited control fidelity, which might have no other use, for example additional nuclear spins surrounding an NV center or other defect centers; and (4) the decision to apply the gates and/or measurements needed to use the spectator information can be deferred until after the noise has acted. This allows a pre-characterized trade-off between information gain and added disturbance to ensure that each spectator is used only when it improves the final memory fidelity. A potential use-case is in protocols where the quantum state of the memory qubit is teleported away from the node [18], allowing the spectator qubits to be measured afterward without causing additional disturbance of the teleported quantum state. In this work we focused on optimizing the memory-qubit fidelity after a successful, deterministic entanglement distribution, i.e., after success is heralded after a variable number of N_{REA} attempts. In the future, one could also consider probabilistic processes where the memory qubit is discarded if entanglement does not succeed early enough. Note that in such scenarios the trade-offs between memory fidelity, entangled state fidelity and the overall resulting success rates—as well as the corresponding most appropriate figure of merit—are highly specific to the desired application.

In conclusion, we show that spectator qubits can be used in various situations to reduce the dephasing of a quantum-network memory, potentially using already present resources at limited cost. Given that the process itself does not add considerable dephasing, then it is always preferable to obtain information about the noise. This makes spectator qubits a promising avenue for near-term quantum network testbeds, where even modest fidelity enhancements might unlock new capabilities.

ACKNOWLEDGMENTS

We acknowledge M. Markham and D. J. Twitchen for supplying the sample. We want to thank B. Terhal for useful discussions. This publication is part of the QuTech NWO funding 2020–2024—Part I "Fundamental Research" with Project No. 601.QT.001-1, which is financed by the Dutch Research Council (NWO). This work is supported by German Federal Ministry of Education and Research (BMBF) for the project QECHQS with Grant No. 16KIS1590K. This work was supported by the Netherlands Organisation for Scientific Research (NWO/OCW) through a Vidi grant (680-47-552). This project has received funding from the European Research Council (ERC) under the European Union's Horizon 2020 research and innovation programme (Grant Agreement No. 852410).

S.J.H.L., Y.W. and T.H.T. devised the project and experiments. S.J.H.L. took and analyzed all experimental data with input from T.H.T. and Y.W. Y.W. conceived the original idea with proof-of-principle theory calculations and simulations. S.J.H.L. developed the theoretical framework to understand and fit the experimental data. N.D. established the simulation framework applied to the experimental data, on which S.J.H.L. expanded. C.E.B. assisted in analyzing data and taking preliminary data. S.J.H.L. wrote the manuscript with input from all authors. T.H.T. supervised the project.

DATA AVAILABILITY

Data and code that support the findings of this article, and which can be used to reproduce the figures in this manuscript are openly available [42].

[1] S. Wehner, D. Elkouss, and R. Hanson, Quantum internet: A vision for the road ahead, Science **362**, eaam9288 (2018).
[2] L. Jiang, J. M. Taylor, A. S. Sørensen, and M. D. Lukin, Distributed quantum computation based on small quantum registers, Phys. Rev. A **76**, 062323 (2007).
[3] N. H. Nickerson, Y. Li, and S. C. Benjamin, Topological quantum computing with a very noisy network and local error rates approaching one percent, Nat. Commun. **4**, 1756 (2013).
[4] N. H. Nickerson, J. F. Fitzsimons, and S. C. Benjamin, Freely scalable quantum technologies using cells of 5-to-50 qubits with very lossy and noisy photonic links, Phys. Rev. X **4**, 041041 (2014).
[5] Y. Wang, S. Simsek, T. M. Gatterman, J. A. Gerber, K. Gilmore, D. Gresh, N. Hewitt, C. V. Horst, M. Matheny, T. Mengle, B. Neyenhuis, and B. Criger, Fault-tolerant one-bit addition with the smallest interesting color code, Sci. Adv. **10**, eado9024 (2024).
[6] H. J. Kimble, The quantum internet, Nature **453**, 1023 (2008).
[7] M. Pompili, S. L. N. Hermans, S. Baier, H. K. C. Beukers, P. C. Humphreys, R. N. Schouten, R. F. L. Vermeulen, M. J. Tiggelman, L. dos Santos Martins, B. Dirkse, S. Wehner, and R. Hanson, Realization of a multinode quantum network of remote solid-state qubits, Science **372**, 259 (2021).

[8] C. T. Nguyen, D. D. Sukachev, M. K. Bhaskar, B. Machielse, D. S. Levonian, E. N. Knall, P. Stroganov, R. Riedinger, H. Park, M. Lončar, and M. D. Lukin, Quantum network nodes based on diamond qubits with an efficient nanophotonic interface, Phys. Rev. Lett. **123**, 183602 (2019).

[9] C. Babin *et al.*, Fabrication and nanophotonic waveguide integration of silicon carbide colour centres with preserved spin-optical coherence, Nat. Mater. **21**, 67 (2021).

[10] D. D. Awschalom, R. Hanson, J. Wrachtrup, and B. B. Zhou, Quantum technologies with optically interfaced solid-state spins, Nat. Photonics **12**, 516 (2018).

[11] Y. Wang, Using spins in diamond for quantum technologies, Ph.D. thesis, Delft University of Technology, 2023.

[12] H. Bernien, B. Hensen, W. Pfaff, G. Koolstra, M. S. Blok, L. Robledo, T. H. Taminiau, M. Markham, D. J. Twitchen, L. Childress, and R. Hanson, Heralded entanglement between solid-state qubits separated by three metres, Nature **497**, 86 (2013).

[13] P. C. Humphreys, N. Kalb, J. P. J. Morits, R. N. Schouten, R. F. L. Vermeulen, D. J. Twitchen, M. Markham, and R. Hanson, Deterministic delivery of remote entanglement on a quantum network, Nature **558**, 268 (2018).

[14] C. E. Bradley, J. Randall, M. H. Abobeih, R. C. Berrevoets, M. J. Degen, M. A. Bakker, M. Markham, D. J. Twitchen, and T. H. Taminiau, A ten-qubit solid-state spin register with quantum memory up to one minute, Phys. Rev. X **9**, 031045 (2019).

[15] R. Stockill, M. J. Stanley, L. Huthmacher, E. Clarke, M. Hugues, A. J. Miller, C. Matthiesen, C. Le Gall, and M. Atatüre, Phase-tuned entangled state generation between distant spin qubits, Phys. Rev. Lett. **119**, 010503 (2017).

[16] L. J. Stephenson, D. P. Nadlinger, B. C. Nichol, S. An, P. Drmota, T. G. Ballance, K. Thirumalai, J. F. Goodwin, D. M. Lucas, and C. J. Ballance, High-rate, high-fidelity entanglement of qubits across an elementary quantum network, Phys. Rev. Lett. **124**, 110501 (2020).

[17] C. M. Knaut, A. Suleymanzade, Y.-C. Wei, D. R. Assumpcao, P.-J. Stas, Y. Q. Huan, B. Machielse, E. N. Knall, M. Sutula, G. Baranes, N. Sinclair, C. De-Eknamkul, D. S. Levonian, M. K. Bhaskar, H. Park, M. Lončar, and M. D. Lukin, Entanglement of nanophotonic quantum memory nodes in a telecom network, Nature **629**, 573 (2024).

[18] S. L. N. Hermans, M. Pompili, H. K. C. Beukers, S. Baier, J. Borregaard, and R. Hanson, Qubit teleportation between non-neighbouring nodes in a quantum network, Nature **605**, 663 (2022).

[19] S. de Bone, P. Möller, C. E. Bradley, T. H. Taminiau, and D. Elkouss, Thresholds for the distributed surface code in the presence of memory decoherence, AVS Quantum Sci. **6**, 033801 (2024).

[20] C. E. Bradley, S. W. de Bone, P. F. W. Möller, S. Baier, M. J. Degen, S. J. H. Loenen, H. P. Bartling, M. Markham, D. J. Twitchen, R. Hanson, D. Elkouss, and T. H. Taminiau, Robust quantum-network memory based on spin qubits in isotopically engineered diamond, npj Quantum Inf. **8**, 122 (2022).

[21] A. Faraon, P. E. Barclay, C. Santori, K.-M. C. Fu, and R. G. Beausoleil, Resonant enhancement of the zero-phonon emission from a colour centre in a diamond cavity, Nat. Photonics **5**, 301 (2011).

[22] M. Ruf, M. J. Weaver, S. B. van Dam, and R. Hanson, Resonant excitation and Purcell enhancement of coherent nitrogen-vacancy centers coupled to a Fabry-Perot microcavity, Phys. Rev. Appl. **15**, 024049 (2021).

[23] D. M. Lukin, C. Dory, M. A. Guidry, K. Y. Yang, S. D. Mishra, R. Trivedi, M. Radulaski, S. Sun, D. Vercruysse, G. H. Ahn, and J. Vučković, 4H-silicon-carbide-on-insulator for integrated quantum and nonlinear photonics, Nat. Photonics **14**, 330 (2020).

[24] H. K. C. Beukers, Improving coherence of quantum memory during entanglement creation between nitrogen-vacancy centres in diamond, M.Sc. thesis, TU Delft, RUG University, 2019.

[25] A. Reiserer, N. Kalb, M. S. Blok, K. J. M. van Bemmelen, T. H. Taminiau, R. Hanson, D. J. Twitchen, and M. Markham, Robust quantum-network memory using decoherence-protected subspaces of nuclear spins, Phys. Rev. X **6**, 021040 (2016).

[26] H. P. Bartling, M. H. Abobeih, B. Pingault, M. J. Degen, S. J. H. Loenen, C. E. Bradley, J. Randall, M. Markham, D. J. Twitchen, and T. H. Taminiau, Entanglement of spin-pair qubits with intrinsic dephasing times exceeding a minute, Phys. Rev. X **12**, 011048 (2022).

[27] S. Majumder, L. Andreta de Castro, and K. R. Brown, Real-time calibration with spectator qubits, npj Quantum Inf. **6**, 19 (2020).

[28] J. L. Orrell and B. Loer, Sensor-assisted fault mitigation in quantum computation, Phys. Rev. Appl. **16**, 024025 (2021).

[29] K. Singh, C. E. Bradley, S. Anand, V. Ramesh, R. White, and H. Bernien, Mid-circuit correction of correlated phase errors using an array of spectator qubits, Science **380**, 1265 (2023).

[30] A. Lingenfelter and A. A. Clerk, Surpassing spectator qubits with photonic modes and continuous measurement for Heisenberg-limited noise mitigation, npj Quantum Inf. **9**, 81 (2023).

[31] R. S. Gupta, L. C. G. Govia, and M. J. Biercuk, Integration of spectator qubits into quantum computer architectures for hardware tune-up and calibration, Phys. Rev. A **102**, 042611 (2020).

[32] A. Youssry, G. A. Paz-Silva, and C. Ferrie, Noise detection with spectator qubits and quantum feature engineering, New J. Phys. **25**, 073004 (2023).

[33] H. Song, A. Chantasri, B. Tonekaboni, and H. M. Wiseman, Optimized mitigation of random-telegraph-noise dephasing by spectator-qubit sensing and control, Phys. Rev. A **107**, L030601 (2023).

[34] B. Tonekaboni, A. Chantasri, H. Song, Y. Liu, and H. M. Wiseman, Greedy versus map-based optimized adaptive algorithms for random-telegraph-noise mitigation by spectator qubits, Phys. Rev. A **107**, 032401 (2023).

[35] M. H. Abobeih, Y. Wang, J. Randall, S. J. H. Loenen, C. E. Bradley, M. Markham, D. J. Twitchen, B. M. Terhal, and T. H. Taminiau, Fault-tolerant operation of a logical qubit in a diamond quantum processor, Nature **606**, 884 (2022).

[36] M. S. Blok, N. Kalb, A. Reiserer, T. H. Taminiau, and R. Hanson, Towards quantum networks of single spins: Analysis of a quantum memory with an optical interface in diamond, Faraday Discuss. **184**, 173 (2015).

[37] M. H. Abobeih, J. Randall, C. E. Bradley, H. P. Bartling, M. A. Bakker, M. J. Degen, M. Markham, D. J. Twitchen, and

T. H. Taminiau, Atomic-scale imaging of a 27-nuclear-spin cluster using a quantum sensor, Nature **576**, 411 (2019).

[38] See Supplemental Material at http://link.aps.org/supplemental/10.1103/zgm8-6b8l, which includes Refs. [43–46].

[39] N. Kalb, P. C. Humphreys, J. J. Slim, and R. Hanson, Dephasing mechanisms of diamond-based nuclear-spin memories for quantum networks, Phys. Rev. A **97**, 062330 (2018).

[40] S. L. N. Hermans, M. Pompili, L. D. Santos Martins, A. R.-P. Montblanch, H. K. C. Beukers, S. Baier, J. Borregaard, and R. Hanson, Entangling remote qubits using the single-photon protocol: An in-depth theoretical and experimental study, New J. Phys. **25**, 013011 (2023).

[41] A. J. Stolk *et al.*, Metropolitan-scale heralded entanglement of solid-state qubits, Sci. Adv. **10**, eadp6442 (2024).

[42] S. J. H. Loenen, Y. Wang, N. Demetriou, C. E. Bradley, T. H. Taminiau, Data and simulations underlying the research article "Quantum-Network Nodes With Real-Time Noise Mitigation Using Spectator Qubits", https://doi.org/10.4121/3929b39b-06e7-45c3-967a-6801e2ea3ae1.

[43] B. M. Terhal and D. Weigand, Encoding a qubit into a cavity mode in circuit QED using phase estimation, Phys. Rev. A **93**, 012315 (2016).

[44] D. W. Berry, H. M. Wiseman, and J. K. Breslin, Optimal input states and feedback for interferometric phase estimation, Phys. Rev. A **63**, 053804 (2001).

[45] L. Robledo, L. Childress, H. Bernien, B. Hensen, P. F. A. Alkemade, and R. Hanson, High-fidelity projective readout of a solid-state spin quantum register, Nature **477**, 574 (2011).

[46] J. Cramer, N. Kalb, M. A. Rol, B. Hensen, M. S. Blok, M. Markham, D. J. Twitchen, R. Hanson, and T. H. Taminiau, Repeated quantum error correction on a continuously encoded qubit by real-time feedback, Nat. Commun. **7**, 11526 (2016).